Research Article | Vol. 28, No. 18 / 31 August 2020 / Optics Express 26122
Optics EXPRESS

Exploiting optical nonlinearities for group delay dispersion compensation in femtosecond optical parametric oscillators

IGNAS STASEVIČIUS[1,2,*] AND MIKAS VENGRIS[1,2]

[1] Vilnius University Laser Research Center, Saulėtekio av. 10, LT-10223 Vilnius, Lithuania
[2] Light Conversion, Keramikų 2b, Vilnius LT-10223, Lithuania
[*] ignas.stasevicius@lightcon.com

Abstract: A wavelength tunable femtosecond optical parametric oscillator pumped by the second harmonic of a Yb: KGW solid state oscillator was investigated. The intracavity group delay dispersion was positive, and soliton condition was satisfied by introducing negative nonlinearity from cascaded quadratic nonlinearity (CQN). Two different approaches were investigated – CQN induced by the same amplifying nonlinear crystal or CQN induced by an additional second harmonic generating nonlinear crystal inside the same resonator. The second crystal was shown to correct the resonator misalignment induced by the rotation of the amplifying crystal as the wavelength was tuned in the range of 770-970 nm. It simultaneously compensated positive resonator GDD offsets of +/- 1000 fs^2 with +/- 5% SHG power losses, simulating a method for compensation of GDD ripples in a broadband mirror.

© 2020 Optical Society of America under the terms of the OSA Open Access Publishing Agreement

1. Introduction

Synchronously pumped femtosecond optical parametric oscillators (OPOs) are tunable wavelength laser sources invaluable in multiphoton and nonlinear microscopy. Broad tuning range, high output power and pulse repetition rate, parameter flexibility, low-noise, small footprint and low cost are the main requirements for an ideal light source for nonlinear microscopy. The light sources where all these features are combined in a single package are still lacking. In order to further their development, we have investigated a novel approach of soliton generation in a simple all-positive-dispersion femtosecond OPO pumped by the second harmonic of Yb:KGW femtosecond oscillator. High intracavity intensity of OPOs leads to self-phase modulation (SPM) induced spectral broadening which usually needs to be compensated by negative group delay dispersion (GDD) created by a prism pair [1,2] or chirped mirrors [3,4]. Design of broadband chirped mirrors is complicated, because increasing the bandwidth leads to lower reflection coefficient and larger GDD oscillations across the spectrum. Such GDD irregularities have a negative impact on pulse duration, power and spectral characteristics of the OPO output [5]. On the other hand, GDD compensator employing a prism pair requires large physical separation between the prisms, resulting in a larger device footprint. A novel approach of SPM compensation is to use a negative cascaded quadratic nonlinearity (CQN). The CQN is a nonlinear process, whereby a wave experiences a nonlinear conversion to a different frequency (travelling at different phase velocity) and a subsequent back-conversion to the original frequency. As a net result, the frequency of the wave remains unchanged, but the wave experiences an effective phase shift (delay), compared to purely linear propagation. This process is equivalent to the propagation in the medium with nonlinear refractive index proportional to $d_{eff}^2/\Delta k$, hence allowing to control the sign of the nonlinearity by changing the detuning Δk [6]. Nonlinear CQN-induced phase shifts experienced by pulses in difference frequency generation (DFG) and second harmonic generation (SHG) have opposite signs [7,8]. Negative CQN was exploited in a comb generation [9], supercontinuum generation [10,11], CW pumped optical parametric oscillators [12] and

#399083 https://doi.org/10.1364/OE.399083
Journal © 2020 Received 1 Jun 2020; revised 17 Jul 2020; accepted 25 Jul 2020; published 20 Aug 2020

Optics EXPRESS

ultrafast laser oscillators with varying levels of pulse energies [13–17]. The evidence of the CQN impact to pulse characteristics was also observed in the femtosecond optical parametric oscillators while operating with negative and positive group delay dispersion in a soliton regime, but a more detailed investigation is still lacking [18,19]. In our previous work we have investigated the CQN influence to pulse and spectrum characteristics while operating with the negative resonator GDD. The results showed SPM distorted spectra with negative nonlinearity and soliton-like behaviour with positive nonlinearity [8]. In this paper, we demonstrate the exploitation of CQN in a wavelength tunable femtosecond optical parametric oscillator while operating with a positive group velocity dispersion in a soliton regime.

Three series of experiments were performed. In the first series A) the CQN was induced by changing the phase matching angle of the OPO crystal, i.e. running OPO at non-optimal conversion efficiency. In addition to lower efficiency, another drawback of this method is the fact that amplification and negative CQN are coupled and independent control of both parameters cannot be achieved. We did observe soliton-like pulses with low time bandwidth product even below the first soliton energy threshold. This effect was ascribed to temporal domain filtering with short duration synchronous pump pulses, as shown in [8]. In the second group of experiments B), an additional doubling crystal was placed in the second intracavity focus. The second nonlinear crystal was cut for frequency doubling the signal wave, and the phase matching was detuned to low conversion efficiency. Contrary to the first series of experiments, the OPO crystal was now exactly phase matched and the OPO was operated at optimal conversion efficiency. This configuration allowed independent control of amplification and negative CQN parameters. Finally, in the third series of experiments C), we demonstrated the wavelength tuning characteristics of all positive dispersion femtosecond optical parametric oscillator with two negative CQN methods – either rotating OPO crystal, or SHG crystal.

2. Experimental procedures

The optical setup used in the experiments is shown in Fig. 1. The optical parametric oscillator is pumped by the second harmonic of Yb: KGW based femtosecond oscillator (Flint, Light Conversion). The pump oscillator emits 12 W of output power with 140 fs pulse duration at 1030 nm center wavelength and 76 MHz repetition rate. The pump light is frequency doubled in 2.5 mm length LBO crystal with AR coatings (1030 + 515 nm), where 6 W of output power at 515 nm is generated with 50% conversion efficiency. The pulse duration of the 515 nm light is 135 fs. The fundamental light is filtered out and the 515 nm beam is delivered to the OPO crystal. The pump light is focused to the spot size of 50 μm (radius $1/e^2$) to match the resonating mode's radius. The cavity design includes the second focus, where CQN crystal can be placed. The calculated mode radius in the second focus is the same as in the amplifying crystal with the spot size of 50 μm (radius $1/e^2$). Cavity mirrors M7, M8, M9, M10 are high reflective in the range from 770 nm to 970 nm, the used mirror design is a simple λ/4 stack with a low group velocity dispersion through the wavelength range (decreasing from +20 fs^2 at 770 nm to −20 fs^2 at 970 nm). The used concave mirrors (M5, M6, M7, M8 with radius R = −200 mm) focus the resonating beam in the nonlinear crystals. Mirrors M5, M6 were highly reflective in 770-970 nm range with high transmission at 515 nm and a similar group velocity dispersion as the plane mirrors. The output coupler OC has 10% of transmission in the wavelength range of 770-970 nm. Multiple fused silica windows (GP1, 14 mm thickness, AR coated for 650-1000 nm, R<0.5%) allowed to coarsely vary the positive group velocity dispersion of the resonator. In most experiments with fixed resonator GDD, two fused silica glass plates were used and the total calculated group delay dispersion of the cavity was ~1800 fs^2 at 860 nm. In the GDD tuning experiments, up to 7 fused silica plates (GP1) were inserted into the cavity to allow the maximum GDD value of 5500 fs^2 at 860 nm. Up to 2 fused silica windows (GP2, 3.5 mm thickness, AR coated for 650-1000 nm, R<0.5%) were inserted intracavity to finely vary positive group velocity dispersion of the

Optics EXPRESS

resonator. To keep the resonator losses the same with varying number of intracavity glass plates, a 0.5 mm thick uncoated Fused Silica glass plate BP was rotated out of the Brewster's angle to induce additional reflection losses, which were measured by power meter. The OPO crystal was a 2.5 mm thick LBO (type I, θ=14°, Eksma Optics). The crystal was AR coated at 1030 + 515 nm. In the second and third part of the experiments, an additional 0.7 mm thick BBO crystal was used in the second focus (type I, θ=24°, Eksma Optics). The crystal was AR coated at 1030 + 515 nm. The reflection coefficient at the signal wavelength range 770-970 nm was experimentally measured to vary from 2.5% (770 nm) to 1% (970 nm) for BBO and from 5% (770 nm) to 2% (970 nm) for LBO. Both crystals were mounted on precision rotation stages allowing the control of the phase matching angle, which was later recalculated to internal angle. In order to minimize the effect of crystal tilt on the cavity alignment, the resonator stability was optimized for the lowest misalignment sensitivity, following ABCDEF matrix formalism calculations [20,21]. The misalignment sensitivities for rotation of both crystals were calculated to be similar in magnitude, and the crystals were rotated in opposite directions to keep the output beam position unchanged during tuning. Nevertheless, the pump beam direction had to be slightly adjusted during this procedure indicating, that the compensation was not exact. Beam dump discarded the remaining pump and idler beams and the second harmonic of the signal beam after the second pass through the BBO crystal. The power of the doubled signal beam power was measured after the first pass through the BBO crystal. The coatings of M8 mirror were not optimized for UV transmission, the transmission was measured to be 70% at 430 nm and the measured power was recalibrated. OPO cavity length was adjusted by moving the output coupler placed on a translation stage, to enable synchronous pumping conditions. The movement of translation table is also used to stabilize the central wavelength of OPO generation. Ambient temperature deviations lead to the pump and OPO resonators' length changes. For OPO to generate, the synchronous pumping condition has to be always satisfied. Under small temperature changes, the generation shifts to signal wavelengths with larger or smaller group velocities, determined by the cavity GDD. So the center wavelength is used as a feedback signal for the movement of the translation table.

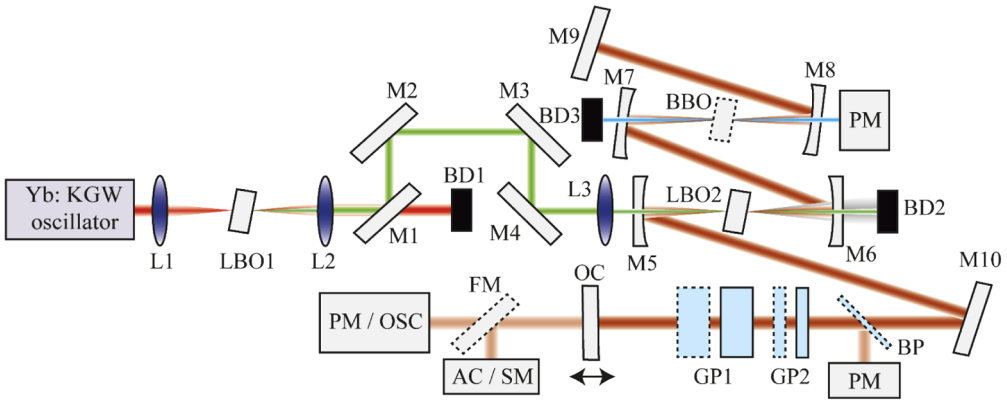

Fig. 1. Experimental setup. L1, L2, L3 – lenses for second harmonic generation, collimation and pump light focusing respectively. M1, M2, M3, M4 – mirrors for pump light delivery with high transmission at fundamental wavelength. M5, M6, M7, M8 – curved resonator mirrors. M9, M10 – plane resonator mirrors. OC – output coupler on a translation stage. LBO1 – second harmonic crystal. LBO2 – intracavity LBO crystal on a rotation stage. BBO – intracavity BBO crystal on a rotation stage used in experiment parts B) and C). GP1, GP2 intracavity fused silica glass plates. BP – intracavity fused silica glass plate near to Brewster's angle. BD1, BD2, BD3 – beam dump. FM – flip mirror. PM – power meter, OSC – oscilloscope, AC – autocorrelator, SM – spectrometer.

Optics EXPRESS

When phase mismatch is induced either with OPO or SHG crystals, the beam quality is not changed if resonator is operated in the center of the $(A + D)/2$ stability parameter range, with a stable zone defined as a $-1 < (A + D)/2 < 1$. When operated near the resonator's stability edge with $(A + D)/2 \sim +-1$, the resonator is sensitive to the spatial focusing / defocusing induced by the CQN. This leads to the change of resonator's mode size. The detailed analysis of spatial effects will be presented in a separate study (in preparation). In the remainder of the experiments, we have operated the resonator at the center of the $(A + D)/2$ parameter stability range with $(A + D)/2 \sim 0$ for both coordinates, where the spatial distortions of the mode due to CQN are minimal.

Average power of the output radiation was measured using a power meter (Nova-2, Ophir) with a thermopile detector (30(150)A-BB-18, Ophir). Spectra were recorded using a spectrometer (STS-NIR, Ocean Optics), pulse durations were measured using scanning autocorrelator (Geco, Light Conversion), and the pulse trains were measured with a photodiode (DET10A2, Thorlabs) connected to an oscilloscope (TDS 3054, Tektronix).

3. Numerical modelling

To allow better physical interpretations of the experimental data, we employed an OPO model where two sets of coupled nonlinear equations are solved. During the single intracavity crystal experiment, optical parametric amplification equations are solved given by equations (1) to (3). When two intracavity crystals are used, optical parametric amplification equations (1) to (3) and second harmonic generation equations of the signal (4)-(5) are solved [22,23].

$$\frac{\partial E_i}{\partial z} + v_{is}\frac{\partial E_i}{\partial t} - \frac{i}{2}k_i''\frac{\partial^2 E_i}{\partial t^2} = -i\sigma_i E_s^* E_p e^{-i\Delta k_{OPO} z} - i\beta_i E_i\left(|E_i|^2 + \gamma_{is}|E_s|^2 + \gamma_{ip}|E_p|^2\right), \quad (1)$$

$$\frac{\partial E_s}{\partial z} - \frac{i}{2}k_s''\frac{\partial^2 E_s}{\partial t^2} = -i\sigma_s E_i^* E_p e^{-i\Delta k_{OPO} z} - i\beta_s E_s\left(|E_s|^2 + \gamma_{is}|E_i|^2 + \gamma_{sp}|E_p|^2\right), \quad (2)$$

$$\frac{\partial E_p}{\partial z} + v_{ps}\frac{\partial E_p}{\partial t} - \frac{i}{2}k_p''\frac{\partial^2 E_p}{\partial t^2} = -i\sigma_p E_i E_s e^{i\Delta k_{OPO} z} - i\beta_p E_p\left(|E_p|^2 + \gamma_{ip}|E_i|^2 + \gamma_{sp}|E_s|^2\right), \quad (3)$$

$$\frac{\partial E_s}{\partial z} - \frac{i}{2}k_s''\frac{\partial^2 E_s}{\partial t^2} = -i\sigma_s E_s^* E_{SH} e^{-i\Delta k_{SHG} z} - i\beta_s E_s\left(|E_s|^2 + \gamma_{SHs}|E_{SH}|^2\right), \quad (4)$$

$$\frac{\partial E_{SH}}{\partial z} + v_{SHs}\frac{\partial E_{SH}}{\partial t} - \frac{i}{2}k_{SH}''\frac{\partial^2 E_{SH}}{\partial t^2} = -i\frac{\sigma_{SH}}{2}E_s^2 e^{i\Delta k_{SHG} z} - i\beta_{SH}E_{SH}\left(|E_{SH}|^2 + \gamma_{SHs}|E_s|^2\right). \quad (5)$$

Electric fields E_i, E_p, E_s are the electric field amplitudes of idler, pump and signal respectively. Electric field E_{SH} is the electric field of the double frequency signal second harmonic. The equations are solved by split-step method in the signal frame of reference, where v_{is}, v_{ps}, v_{SHs} are the group velocity mismatches of signal-idler, signal-pump and signal-signal second harmonic respectively. Group velocity dispersion coefficient is denoted as $k''_{i,s,p,SH}$, $\sigma_{i,s,p,SH}$ are nonlinear coupling coefficients, $\beta_{i,s,p,SH}$ self-phase modulation coefficient, $\gamma_{is,ip,sp,SHs}$ cross-phase modulation coefficient for idler, signal, pump and frequency doubled signal, as given by indices. The definition of the nonlinear coupling, self- and cross-phase modulation coefficients are given in [22]. The nonlinear refractive indices and effective nonlinearities could all be found in [24]. Difference frequency induced phase mismatch Δk_{OPO} is defined as $\Delta k_{OPO} = k_p - k_s - k_i$ and the second harmonic generation induced phase mismatch Δk_{SHG} is defined as $\Delta k_{SHG} = k_{SH} - 2k_s$. After each pass through the crystal, the signal pulse is time-delayed, losses and resonator group velocity dispersion are applied. In the simulation of two-crystal experiment, the signal pulse is injected into the second harmonic crystal and the equations are again solved with split-step method. The second pass is solved with a new second harmonic wave with 1% of the first pass

Optics EXPRESS

generated SHG power (result after filtering by three cavity mirrors), as experimentally the signal beam is double passed through the crystal. As the returning pass SHG power is low and the distance propagated in air is small, the spectral phase of the SHG input was assumed to be the same as at the exit of the crystal after the first pass. Afterwards, the signal pulse Eq. (2) is solved in the OPO crystal without pump and idler for the signal SPM only. Finally, the signal pulse is returned to the OPO crystal for another cycle with a new pump pulse. This process is continued until the signal output power saturates, i.e. the resonator losses become equal to the gain. To save computational cost, the coupled equations are solved in time domain only, with spatial effects, such as beam walk-off, excluded. During split-step calculation the crystal was divided into 200 steps to limit the phase shift to less than $\pi/10$ for the highest frequency component of the entire spectrum (670 nm to 1200 nm for signal wavelength). The time domain sampling step was 5 fs with 2560 fs total time window to achieve the desired spectral resolution (~1 nm step size at the simulated signal wavelength). When the OPO operates in a steady-state regime, the signal pulse remains unchanged after a round trip. The ratio of power between consecutive pulses is used as a condition for steady state operation. Program stops, when the standard deviation of power of the last 10 round trips' is smaller than 0.001% of the mean output power. We employ a routine that calculates the OPO central wavelength, spectral bandwidth, pulse duration and output power after each round trip. Additionally, resonator GDD is calculated from linear spectral phase and nonlinear refractive index from nonlinear time domain phase to compare these parameters to experimentally measured ones. The nonlinear phase is induced by nonlinear part of the system of Eqs. (1)–(3) and (4)–(5). During each step of the split step algorithm, this nonlinear part is solved and nonlinear phase shift is extracted independently from linear phase. At end of the crystal, the peak time domain nonlinear phase shift is used for nonlinear refractive index calculation by using a phase relationship $\Delta\varphi_{NL} = k_0 L n_2^{eff} I$, where n_2^{eff} is an effective crystal nonlinear coefficient.

Positive / negative nonlinearity and the corresponding negative / positive resonator group delay dispersion leads to the soliton formation. An integer number of the soliton order parameter $N_{soliton}$ is given by square root of ratio of dispersive length L_D to nonlinear length L_{NL}. Dispersive length is defined as a distance after which pulse duration increases by a factor of $\sqrt{2}$. Nonlinear length is defined as a distance after which accumulated nonlinear phase reaches 1 radian. If the $N_{soliton} < 1$, the pulse evolution is dominated by dispersion, if the $N_{soliton} > 1$, the pulse evolution is dominated by the self-phase modulation. The exact balance with $N_{soliton} = 1$ leads to the fundamental soliton which has a stable pulse and spectrum shape when propagating. Higher integer order $N_{soliton} > 1$ solitons show periodic time and frequency domain oscillations with a soliton period. The pattern of the oscillations becomes more complicated and dominated by SPM with increasing soliton order $N_{soliton}$. The soliton order equation is given by [22]:

$$N_{soliton} = \sqrt{\frac{L_D}{L_{NL}}} = \frac{\tau_0 (k''_{eff})^{-1/2}}{\left(\frac{n_2^{eff}\omega_0}{cA_{eff}} P_0\right)^{-1/2}}. \tag{6}$$

Where τ_0 is pulse duration, P_0 is intracavity peak power, A_{eff} is the effective beam area, c – speed of light in vacuum, ω_0 is angular frequency, k''_{eff} is resonator group velocity dispersion normalized to crystal length. In the case of two crystals, the crystal lengths are averaged using the effective nonlinearities as weighting coefficients. From the Eq. (6), the N-th order soliton FWHM duration and soliton intracavity average power can be calculated [1,13]:

$$\tau_N = -\frac{\lambda k''_{eff} N_{soliton}^2 A_{eff} f}{0.57\,\pi n_2^{eff} P_{ave}}, \tag{7}$$

$$P_N = -\frac{\lambda k''_{eff} N_{soliton}^2 A_{eff} f}{0.57\,\pi n_2^{eff} \tau}. \tag{8}$$

Optics EXPRESS

Here, λ is the signal wavelength and f – pulse repetition rate. Experimentally measured values of the output average power, pulse duration and numerically calculated effective nonlinearity are used in calculation of soliton duration and soliton power given by Eqs. (7) and (8). Using numerical modelling results, nonlinear phase is extracted and soliton order given by Eq. (6) is calculated. When nonlinearity increases, the nonlinear length decreases and an increasing order of soliton can be supported by the cavity as given by Eq. (6). In this paper, the operating regimes are numbered by increasing orders of soliton supported by the cavity – zone 0: from zero negative nonlinearity up to the 1st order soliton; zone I: from 1st up to the 2nd order soliton; zone II: from 2nd to the 3rd order soliton. The color coding of increasing red tone is given to the zones as a visual aid.

4. Results and discussion

4.1. Single nonlinear crystal scheme with DFG CQN

In the first part of the experiments, the OPO crystal is phase mismatched by angle tuning while the center wavelength is fixed at 860 nm. The resonator length is changed for precise wavelength control. The induced cascaded quadratic nonlinearity originates from phase mismatched difference frequency generation. The mode radius in LBO crystal is ω=50 μm and with zero crystal phase mismatch intensity reaches 20 GW/cm^2. The second focus is formed in air with intensity value of 20 GW/cm^2. This intensity is four orders of magnitude below the ionization threshold of air. In addition, nonlinear refractive index of air is four orders of magnitude lower than that of BBO [25]. It can thus be expected that the self-action of the beam propagating in air does not significantly affect the output characteristics of the OPO. In order to explain the measured pulse and spectrum characteristics, the nonlinear phase was computed using the numerical model (Eqs. (1) to (3)) by simulating a single pass through the OPO crystal with varying crystal angles. An input signal pulse was injected with experimentally observed steady state OPO parameters at the center of the tuning curve: pulse duration τ =200 fs and intracavity average power P = 8 W. A single pass optical parametric amplifier (OPA) simulation nonlinear phase was used instead of full OPO model, because it produced more consistent results of nonlinear phase while phase mismatch was changed. In OPO case, the steady state pulse shape changes as phase mismatch is induced and this leads to non-trivial peak time domain nonlinear phase determination. In a single pass OPA case, the signal pulse shape is nearly constant and this leads to easily extractable peak time domain nonlinear phase. As nonlinearity and OPA are coupled, the crystal rotation changes average power and induced nonlinear phase, but we used fixed pulse parameters for the sake of better comparison with double crystal experiment. Two fused silica glass plates (GP1) are inserted into the cavity to ensure positive group delay dispersion, the total calculated resonator GDD is ~1800 fs^2 at 860 nm. The results are shown in Fig. 2(A). The soliton order is calculated by Eq. (6) with fixed dispersive length and nonlinear length calculated from nonlinear phase. The angle is rotated around phase matching angle $\theta_{OPO\ LBO}$ = 12.7^o for wavelength 860 nm. The results show that the cascaded negative nonlinearity range is in the positive crystal angle offset range and its magnitude is ~4 times larger than intrinsic material nonlinearity. Soliton order shows that with a fixed positive group delay dispersion the negative nonlinearity supports 1st order soliton (given by red color coding zone I). In contrast, the CQN of zone 0 only partially compensates positive GDD. Figure 2(B) compares experimentally measured and numerically simulated output spectra. It is evident that lower crystal angles induce positive cascaded nonlinearity which distorts the spectra through self-phase modulation. Larger crystal angles induce negative nonlinearity which, together with positive GDD, produces Gaussian spectra with transform-limited time-bandwidth product (Fig. 2(D)). As spectra are deformed, the bandwidths are calculated using standard deviation 2 σ, which for Gaussian spectrum relates to FWHM as ~2.35 σ. The discrepancy between the measured and numerically simulated spectra could be caused by an overestimated numerical modelling intracavity intensity as spatial mode

Optics EXPRESS

distribution is not accounted for. The overestimated intracavity intensity leads to more severe spectrum distortion caused by the self-phase modulation. The corresponding output power tuning curve and the output pulse durations are presented in Fig. 2(C). The soliton durations and powers, calculated by Eqs. (7) and (8), are plotted as zones in red color coding. The output power is too low and pulse duration is too short to support the 1st order soliton threshold (zone I) with a fixed resonator GDD. Even though numerical simulation reaches the 1st order threshold, it does not show any pronounced differences in power and pulse duration. But as a feature of soliton behaviour the time-bandwith product reaches the minimum ~0.44 value. Using this approach, the time-bandwidth product could be reduced to the value of ~0.55 from ~0.8 with around $\Delta\theta_{OPO\ LBO} = 0.25^o$ angle detuning (or $\Delta k_{OPO}L = -0.5\,\pi$) and average output power of 720 mW, which is around 20% lower compared to the exact phase matching $\Delta k_{OPO}L = 0$. It must be noted that despite non-optimal operation conditions, the pulse durations are decreased from 215 fs to 185 fs and the pulse peak power is only 5% lower compared to the phasematched case.

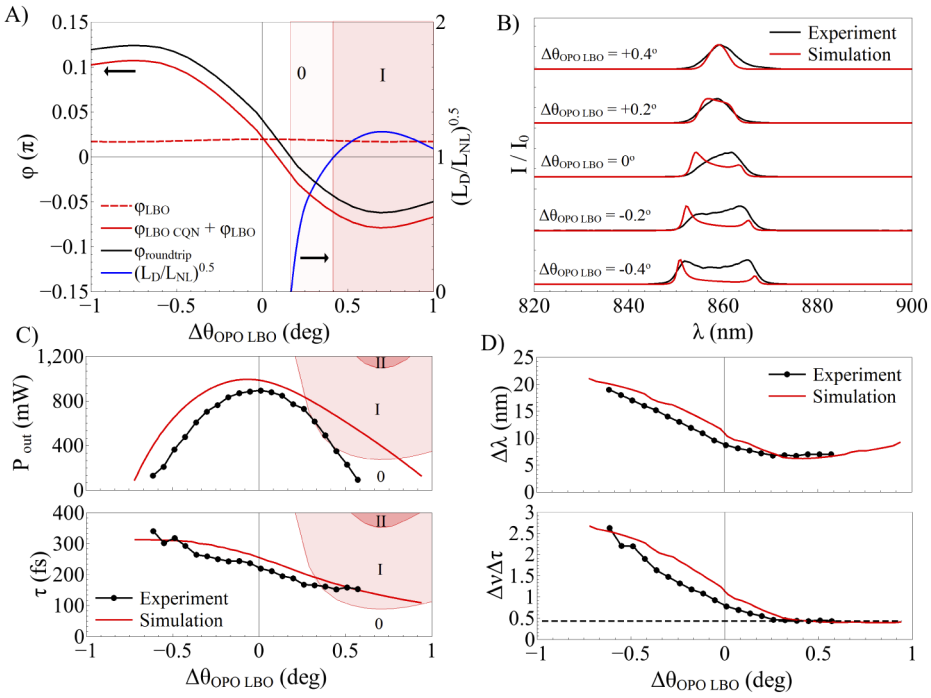

Fig. 2. A) OPO nonlinear phase and soliton number dependence on LBO crystal angle. B) Experimental and simulated spectra when OPO LBO crystal angle is detuned from the exact phase matching at 860 nm. C) Experimental and simulated signal output power and pulse duration dependence on crystal angle. D) Experimental and simulated signal spectrum bandwidth (calculated as 2 σ) and time-bandwidth product dependence on crystal angle, dashed line indicates minimum for gaussian pulses TBP ~ 0.44. In panels A) and C) negative CQN areas (0, I, II) with red color tones indicate output powers / pulse durations large enough to support soliton of corresponding order $N = 0, 1, 2$. In all panels signal center wavelength is fixed at 860 nm.

4.2. *Double nonlinear crystal scheme with SHG CQN*

In the second part of the experiments, an additional nonlinear BBO crystal is inserted in the second focus, where it is used for frequency doubling of the signal wave. The mode size in an additional intracavity focus is the same as in OPO crystal ω=50 μm. Crystal angle is varied to

Optics EXPRESS

control SHG-induced cascaded quadratic nonlinearity. The calculated signal intensity reaches 20 GW/cm^2 in both crystals. The BBO crystal is used for the SHG crystal because of its higher d_{eff} coefficient (~2 pm/V) which induces higher maximum negative cascaded nonlinearity than LBO (~0.78 pm/V). In the meantime, LBO is used as OPO crystal because of its smaller spatial walk-off value and lower nonlinear refractive index ($n_2 \sim 2 \times 10^{-20}$ m^2/W, twice lower than BBO, where $n_2 \sim 4 \times 10^{-20}$ m^2/W [24]). The positive cavity GDD and positive material nonlinearity require that CQN induce negative refraction. In order to operate with as low as possible SHG conversion efficiency (after all, the generated second harmonic of the signal only increases OPO losses), large phase mismatch and short crystal is required as shown in [13]. The shortest signal pulse duration obtained from the part A) experimental setup was 150 fs. Based on this pulse duration, the SHG crystal length was chosen. 150 fs OPO signal pulses have broad enough spectrum to make the local conversion efficiency minimum vanish as minima and maxima are averaged throughout the spectrum amplitudes. This precludes employing the approach of operating the nonlinear crystal in a local conversion efficiency minimum by Keller et al. [13]. The BBO crystal length of 0.7 mm was used, with a length not limited by spatial walk-off $L_{sp\ walkoff} \sim 1.5\,\omega/\rho \sim 1.3$ mm, where ω is beam radius and ρ is extraordinary pump beam walk-off as shown in [8], and group velocity walk-off between fundamental and second harmonic length $L_{gv\ walkoff} = 2\,\tau/(v_{FM}^{-1} - v_{SH}^{-1})$ ~1.9 mm for pulse length of 150 fs. In order to operate at positive resonator GDD, two fused silica glass plates (GP1) are inserted intracavity, and the calculated GDD is ~1900 fs^2 at 860 nm.

The LBO crystal angle was fixed at $\theta_{OPO\ LBO} = 12.7^o$ for the optimal conversion efficiency and $\Delta k_{OPO} L = 0$ for the wavelength of 860 nm. The BBO crystal was rotated to change internal angle +/- 4° around optimal SHG angle $\theta_{SHG\ BBO} = 27.3^o$ for 860 nm to 430 nm wavelength generation. The center wavelength was fixed at 860 nm by changing the resonator length as SHG BBO crystal was adjusted. The resonator was realigned after each adjustment of the crystal angle for the optimal output power. In order to explain the observed characteristics of the pulse, the nonlinear phase was computed using the numerical model (Eqs. (1) to (5)) by simulating a single pass through the SHG / OPA crystals with varying crystals' angles. An input signal pulse was injected with experimentally observed steady state OPO parameters at the center of the tuning curve: pulse duration τ =200 fs and intracavity average power P = 8 W. The results are given in Fig. 3(A). The soliton order is calculated by Eq. (6) with a fixed dispersive length and a nonlinear length calculated from the nonlinear phase. The soliton order shows that with a fixed positive group delay dispersion the negative nonlinearity supports the formation of solitons up to the 2$^{\text{nd}}$ order. Higher order soliton threshold was not reached because the increase in SHG conversion efficiency decreases the intracavity signal power. The results show that the cascaded negative nonlinearity is in the negative crystal angle offset range and its single pass peak magnitude is ~8 times larger than intrinsic (cubic) material nonlinearity. Operating the crystal in double pass increases the induced negative nonlinearity two-fold with a cost of two-fold increased losses.

The measured signal output power and pulse duration are shown in Fig. 3(C). The nonlinear phase is used for the N-th order soliton power calculation with fixed experimentally measured pulse duration τ =200 fs given by Eq. (8) and N-th order soliton duration calculation with fixed experimentally measured intracavity average power P = 8 W given by Eq. (7). The main dip at the center of power tuning curve is induced by the SHG losses. The increase of the output power at the zone II angle $\Delta\theta_{SHG\,BBO} = -0.3^o$ ($\Delta k_{OPO} L = 4\,\pi$) could be explained by higher pulse energy supported by higher order soliton as given by Eq. (8). Figure 3(B) compares the experimentally measured and numerically simulated output spectra. Contrary to the single crystal detuning case, the lower crystal angles induce negative cascaded nonlinearity which balances the cavity group delay dispersion and produces the bandwidth-limited pulses. The discrepancy between measured and numerically simulated spectra could be attributed to the overestimation of simulated intracavity intensity as spatial domain effects are ignored. The curves of spectral bandwidth and time-bandwidth product in Fig. 3(D) correlate well with the nonlinear phase induced spectrum

Optics EXPRESS

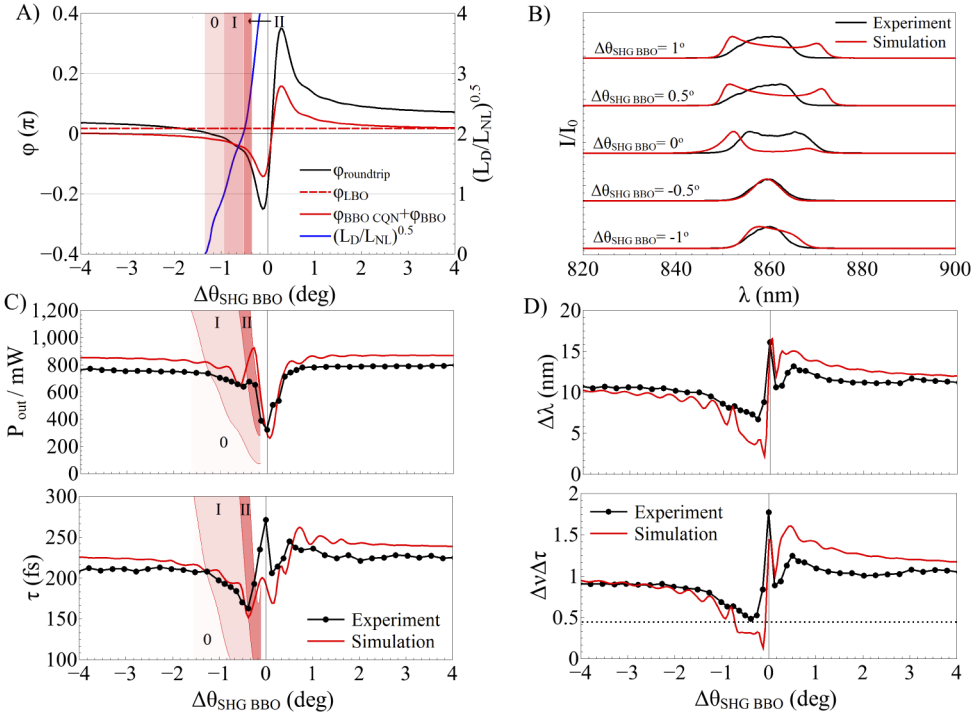

Fig. 3. A) OPO LBO and SHG BBO nonlinear phase and soliton number dependence on SHG BBO crystal angle. B) Experimental and simulated spectra when SHG BBO crystal angle is detuned from the exact second harmonic phase matching at 860 nm. C) Experimental and simulated signal output power and pulse duration dependence on SHG BBO crystal angle. D) Experimental and simulated signal spectrum bandwidth and time-bandwidth product dependence on SHG BBO crystal angle. Dashed line indicates minimum for Gaussian pulses TBP~0.44. In panels A) and C) negative CQN areas (0, I, II) with red color tones indicate crystal angles with negative CQN high enough to support soliton of corresponding order $N = 0, 1, 2$. In all panels signal center wavelength is fixed at 860 nm and OPO LBO angle is fixed at 12.7° for optimal conversion efficiency to 860 nm.

narrowing and pulse duration decrease. At the exact phase matching angle these parameters suddenly increase again because the spectrum of the pulse becomes distorted. Figure 4 shows the single pass signal second harmonic wave power as BBO crystal angle is changed. The SHG power curve shifts to negative crystal angle detunings, because the OPO output power increases at negative crystal offsets. The optimal point is attributed to be $\Delta\theta_{SHG\,BBO} = -0.6^o$ ($\Delta k_{SHG}L = 8\pi$) at the end of zone I (up to the 2nd order soliton formation threshold, zone II). The characteristics of this point can be compared to the case when BBO induces negative nonlinearity equal to its material nonlinearity $\Delta\theta_{SHG\,BBO} = -3.8^o$ ($\Delta k_{SHG}L = 48\pi$), so that there is no BBO nonlinear effect. At the optimal point the average output power is ~660 mW, SHG induced power losses are 15%, pulse duration decreases from 210 fs to 180 fs, time-bandwidth product decreases from ~0.98 to ~0.58. In summary, double crystal approach allows to conserve the peak power and the obtained pulses are close to transform limited.

4.3. *Wavelength tuning with DFG and SHG CQN*

In the last part of the experiments, the wavelength tuning is demonstrated with two negative CQN approaches, as shown in parts A) and B). In the first case, single LBO OPO crystal is used

Optics EXPRESS

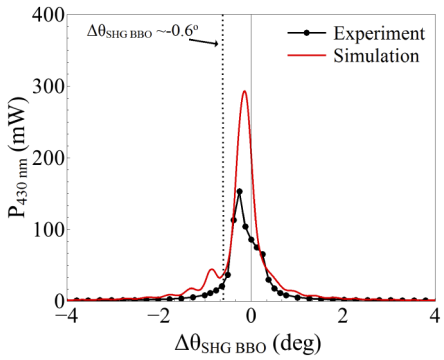

Fig. 4. Experimental and simulated single pass signal second harmonic power, dashed line indicates optimal operating point. Signal center wavelength is fixed at 860 nm and OPO LBO angle is fixed at 12.7° for optimal conversion efficiency to 860 nm.

both as an amplifying medium and a negative DFG CQN source. For the sake of comparison, a 0.5 mm thick fused silica plate is inserted intracavity slightly out of Brewster's angle to induce losses equal to the reflection of SHG BBO crystal at each wavelength. Two intracavity fused silica glass plates (GP1) are inserted to ensure positive resonator GDD, with a roundtrip value of ~ 1800 fs^2. The wavelength is tuned by rotating intracavity LBO crystal. For each wavelength, the LBO crystal angle is offset into negative nonlinearity range for the time-bandwidth product <0.6 with as high as possible conversion efficiency. In the second case, LBO OPO crystal is used as an amplifying medium and a SHG BBO crystal as a negative SHG CQN source. The 0.5 mm thickness glass plate is rotated to Brewster's angle and two intracavity fused silica glass plates (GP1) are inserted to ensure positive resonator GDD, with a roundtrip value of ~ 1900 fs^2. The wavelength is tuned by rotating intracavity LBO crystal to ensure the maximum conversion efficiency and negligible LBO induced CQN. For each wavelength, the SHG BBO crystal angle is optimized for the time-bandwidth product <0.6 with as low as possible SHG conversion efficiency.

Figure 5(A) shows the BBO SHG and OPO LBO crystal rotation angles in three experimental modes: a) minimum time-bandwidth product with OPO LBO; b) minimum time-bandwidth product with SHG BBO; c) BBO nonlinear phase equals 0 and LBO is in optimal conversion efficiency. Additionally, a BBO SHG and OPO LBO angles are shown for which the frequency conversion is phase matched. The nonlinear phase is extracted from a numerical simulation of a single pass through the SHG / OPO crystal with varying crystal angles with fixed pulse duration τ =200 fs and fixed intracavity average power P = 6 W. We chose this power value which is 25% lower than in the cases A) and B) to account for the fact that the OPO power drops when tuning away from the optimum wavelength. The reason for this drop is mostly mirror and crystal coatings reflection losses when operating away from the central wavelength. The center wavelength is varied and the SHG / OPO crystal angles are calculated at which the negative nonlinear phase is high enough to reach the N-th order soliton threshold, calculated by Eq. (6). These are named as N zones and plotted in red color coding. As can be seen from the graph, the experimental SHG / OPO angles are in zone 0 / I (supporting 1st order soliton) throughout the entire tuning range.

For SHG BBO, with increasing wavelength the crystal offsets slightly increase. Larger crystal offsets lead to lower values of induced negative CQN to compensate the decreasing cavity GDD (~2200 fs^2 at 770 nm and ~1500 fs^2 at 970 nm, not including the resonator cavity mirrors). For the same reason, OPO LBO crystal offsets slightly decrease. For a given resonator GDD and intracavity intensity, the optimal wavelength average OPO LBO angle crystal offset is attributed

Optics EXPRESS

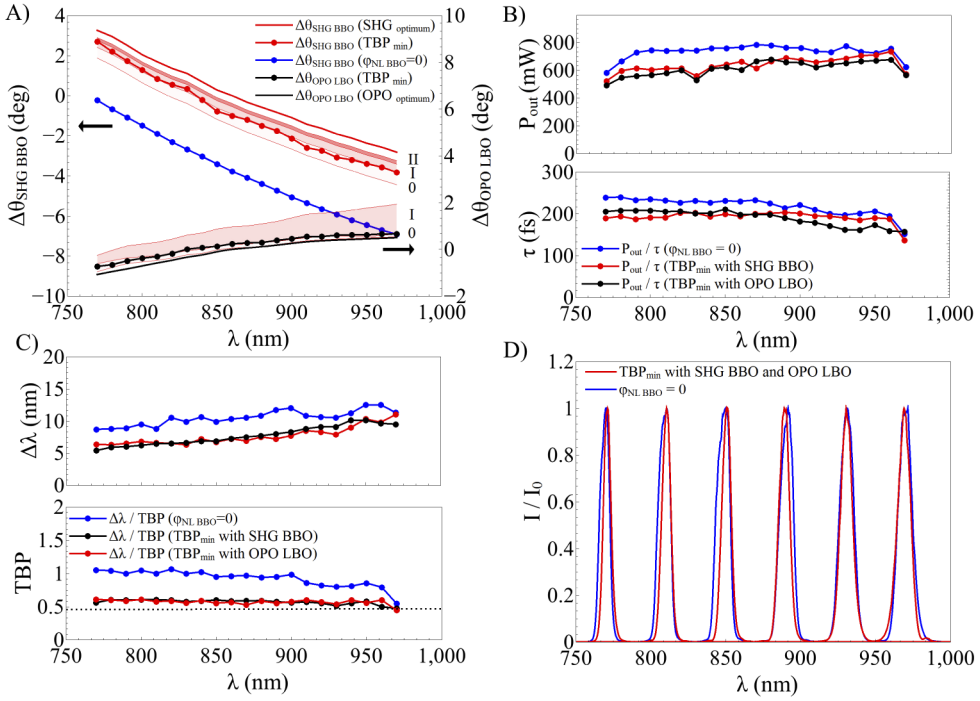

Fig. 5. A) Experimental SHG BBO and OPO LBO internal angle dependence on signal wavelength while the wavelength is tuned. Negative CQN areas (0, I, II) with red color tones indicate SHG BBO and OPO LBO angles with negative CQN high enough to support soliton of corresponding order $N = 0, 1, 2$. B) Output power and pulse duration dependence on signal wavelength while SHG BBO and OPO LBO angles are varied. C) Dependence of signal bandwidth and time-bandwidth product on the signal wavelength at different SHG BBO and OPO LBO crystal angles. Dashed line indicates minimum for Gaussian pulses TBP~0.44. D) Signal spectra while SHG BBO and OPO LBO angles are varied compared to the case without negative CQN. In all panels crystal angles are tuned in three modes – no negative CQN (blue), negative CQN from SHG BBO (red), negative CQN from OPO LBO (black). In panel D) spectra of negative CQN from SHG BBO and negative CQN from OPO LBO overlap and are shown with red color as one line.

to be $\Delta\theta_{OPO\ LBO} = 0.25^o$ (or $\Delta k_{OPO}L = -0.5\,\pi$ at 860 nm). The optimal wavelength average SHG BBO crystal angle offset from the exact phase matching is attributed to be $\Delta\theta_{SHG\ BBO} = -0.6^o$ ($\Delta k_{SHG}L = 8\pi$ at 860 nm). The OPO LBO and SHG BBO $\Delta k_{SHG}L$ sign difference stems from the opposite signs of SHG and DFG CQN induced phase shifts as shown in [7,8].

Figure 5(B) shows the output power and pulse duration of three experimental modes. Up to 25% power losses are induced in the OPO LBO and up to 20% power losses are induced in the SHG BBO cases compared to the power when BBO nonlinear phase equals 0 and LBO is at optimal conversion efficiency. If the optimized AR coatings were used both for LBO and BBO (R<0.25%), the additional BBO crystal reflection losses would decrease the double crystal configuration output power by 10%. On the other hand, the optimal compression SHG losses are 5% smaller than the phase-mismatched OPO LBO power losses. So both set-ups would produce similar output power if optimized AR coatings were used. The compressed pulse durations in both cases are ~ 190 fs compared to the ~ 220 fs when BBO nonlinear phase equals 0, taking an average over the entire investigated spectral range. In other words, the pulses are 15% shorter with close to transform-limited time-bandwidth product; the average peak power is only slightly

Optics EXPRESS

decreased. The spectral bandwidths, TBPs and spectra (which are very similar when compressed either with OPO LBO or SHG BBO) of all three experimental modes are shown in Fig. 5(C) and Fig. 5(D). The uncompressed spectra are broadened and slightly asymmetric, intensity or nonlinearity increase would lead to even more pronounced spectrum deformation induced by SPM as shown in Fig. 2(B).

In order to investigate the limits of compression on the resonator GDD, the intracavity GDD was varied with multiple numbers of fused silica glass plates (GP1-GP2) at a fixed wavelength of 860 nm. To keep resonator losses the same with decreasing number of glass plates, 0.5 mm thickness glass plate was rotated out of Brewster's angle. In Fig. 6(A) top pane the pulse duration dependence on group delay dispersion is shown. As GDD is increased, crystal is detuned to increase the negative CQN both in SHG BBO (smaller detuning, closer to the optimum SHG conversion efficiency) and in OPO LBO (larger detuning, farther away from the optimum OPO conversion efficiency) experimental modes, shown in the bottom pane of Fig. 6(A). In both cases, compensation of the increasing cavity GDD leads to the higher effective resonator losses, in a form of SHG or decreased OPO efficiency. With BBO inducing 0 nonlinear phase, increasing amounts of GDD stretch the signal pulse and short pump pulse acts as a frequency domain filter narrowing the pulse duration. Interplay between the uncompensated SPM and GDD lead to distorted spectrum and large values of time-bandwidth product. When either OPO LBO or SHG BBO crystal is used for negative CQN, the pulse durations decrease through all the positive GDD range, but SHG BBO crystal acts as a better compressor for positive GDD values >2000 fs^2. In order to explain this, the first order soliton duration was calculated by Eq. (7) with a fixed intracavity power of P = 6 W and fixed pulse duration τ =200 fs. Using experimental crystal offsets, the nonlinear phase was calculated from Fig. 2(A) and Fig. 3(A). The SHG BBO soliton pulse duration in Fig. 6(A) shows that the increasing values of the GDD are compensated by negative CQN, which results in a shallower slope of the dependence between the pulse duration and GDD. On the other hand, the LBO OPO soliton pulse duration in Fig. 6(A) shows that the magnitude of the negative CQN is not sufficient to compensate the increasing dispersion. The soliton pulse duration increases linearly vs GDD. Moreover, as the OPO LBO conversion efficiency and negative CQN are inherently coupled, the increase of the negative CQN inhibits short pulse soliton formation because of the decrease of the intracavity power. This explains the pulse duration discrepancy observed in Fig. 5(B) – the SHG BBO compresses the pulses to slightly smaller values with higher values of intracavity GDD (shorter wavelengths), while the OPO LBO compresses the pulses to slightly smaller values with smaller values of intracavity GDD (longer wavelengths).

In a decreasing GDD limit, the shortest pulses we could obtain were around 140 femtoseconds at 860 nm, even though simulated soliton durations reach around 50 fs with 300 fs^2 resonator GDD. We attribute this limit to the dispersive nature of the cascaded nonlinearity. The nonlinear phase oscillation period in a wavelength domain is linked to SHG crystal amplification bandwidth, given by $\Delta\omega = \pi/L_{crystal}/(k'_{SHG} - k'_{SIG})^{-1}$, where k'_{SHG} and k'_{SHG} are the first derivatives of a wavevector at second harmonic and fundamental wavelength. Calculating in wavelength domain at 860 nm the equation results in $\Delta\lambda \sim 12$ nm SHG crystal amplification bandwidth, or 95 fs pulse duration. To further reduce the pulse duration, the crystal should be shortened or the group velocity mismatch between fundamental and second harmonic decreased. Bache et al. have shown that the limits to CQN pulse compression to single-cycle is caused by the fundamental and second harmonic group velocity mismatch [26]. Even though OPO regime is far from single cycle, the parallels of the compression limits could be drawn. The phase mismatch has to be higher than the value of $\Delta k_{sr} = (k'_{SHG} - k'_{SIG})^2/2k''_{SHG}$ to ignore the group velocity mismatch caused oscillatory CQN response. In our case for the SHG BBO exactly phase matched to the wavelength of 860 nm, the Δk_{sr} phase mismatch would correspond to a SHG crystal angle offset of $\Delta\theta_{SHG\,BBO} = -2.9^o$. At this non-phase matched crystal angle the nonlinear phase oscillations

Optics EXPRESS

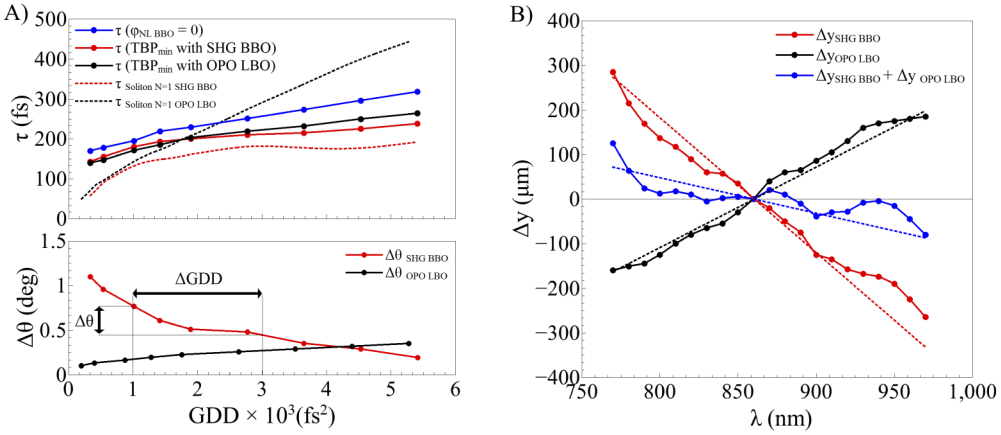

Fig. 6. A) Dependence of signal pulse duration, soliton order N=1 pulse duration and experimental SHG BBO and OPO LBO angle detunings on resonator GDD. ΔGDD indicate the +/- 1000 fs^2 range which is compensated by SHG crystal Δθ. Crystal angles are tuned in three modes – no negative CQN (blue), negative CQN from SHG BBO (red), negative CQN from OPO LBO (black). B) Experimentally measured and calculated (dotted curves) output beam spatial walk off dependence on signal wavelength in three modes - SHG BBO is rotated (red), OPO LBO is rotated (black), both SHG BBO and OPO LBO are rotated simultaneously (blue). In both panes signal wavelength is fixed at 860 nm.

are greatly reduced. On the other hand, at this point with a given OPO intensity reaching ~ 20 GW/cm^2 the negative nonlinearity is too small to compensate the resonator intracavity dispersion and resonator material intrinsic nonlinearity.

One of the practical considerations of the OPO design is misalignment of the optical resonator while a birefringent OPO crystal is rotated. This is especially true for a broadly wavelength tunable source where crystal offsets become larger. In our experimental parts A) and B), while the crystals were rotated, the resonator had to be realigned to keep the output beam in the same position. Figure 6(A) shows the spatial beam walk-offs when the crystals are independently or mutually rotated while the wavelength is changed. The second SHG BBO crystal was inserted with an oppositely orientated crystal axis, so that the rotation would lead to opposite shift of the beam position at the output coupler. In this manner, the simultaneous rotation of both of the crystals leads to the near compensation of the output beam position. As the compensation is not exact, the beam deviates slightly through the tuning range (given by blue curve) and the pump direction has to be slightly aligned for a maximum output power. By using ABCDEF matrix formalism the beam offsets are calculated with experimental crystal lengths, detunings, and resonator parameters. These are shown in Fig. 6(B) with dotted curves. Empirical position offset ratio equation of two foci, two crystal resonator can be derived: $\Delta y_1/\Delta y_2 \sim (L_1\,\Delta\theta_1\,R_2)/(L_2\,\Delta\theta_2\,R_1)$, where L_N, $\Delta\theta_N$, R_N are N crystal length, crystal detuning angle and mirror radius which forms the focus in crystal N. The resonator stability is excluded as its contribution to misalignment sensitivity is equal for both crystal detunings. This equation shows that careful choice of resonator mirror radii and crystal lengths would exactly compensate the output beam position shift ($\Delta y_1/\Delta y_2 = -1$) if detuning angle functions are linear. For the experimentally used crystal rotation ranges, the slopes of the LBO and BBO were similar through the wavelength tuning range. As shown in Fig. 6(A), the compensation of +/- 1000 fs^2 intracavity group delay dispersion around resonator GDD of 2000 fs^2 would require only -/+ 0.17° SHG BBO crystal detuning and would induce only +/- 10 μm beam output position shift. From Fig. 3(B), the SHG BBO crystal offset of -/+ 0.17° would induce additional average power losses of +/- 5%. For comparison, using only OPO LBO

Optics EXPRESS

to compensate +/- 1000 fs^2 at 2000 fs^2 intracavity GDD requires angle detuning of +/- 0.08°, which leads to additional average power losses of +/- 10%. On the other hand, misalignment issue could as well be solved by generating the OPO with temperature tunable periodically poled nonlinear crystals as OPO and SHG pair, which may provide collinear interaction without resonator misalignment [27].

Both these approaches lead to an efficient way to optimize negative nonlinearity, for instance, to the GDD ripples of broad reflection bandwidth intracavity mirror if operating the device with a broad tuning range. For the spectral widths used in our experiment, the third order dispersion (TOD) impact to the spectral phase is really weak, so the uncompensated TOD could be ignored. It is important to emphasize that suitable choice of crystal lengths would allow to compensate both the GDD and the spatial beam offsets in a much broader wavelength range. Operating the BBO crystal as a SHG crystal in a wavelength range of 690-1020 nm would require the crystal internal angle rotation range of $\Delta\theta$ ~10.7°. Simultaneous rotation of LBO crystal as an OPO crystal would require rotation of $\Delta\theta$ ~4°, with the rotation angle ratio being similar to the one in our experiment. The same approach can be transferred to different wavelength ranges as long as the OPO and SHG crystal rotation ranges are quasi-linear through the wavelength range.

5. Conclusions

We have investigated the tuning characteristics of high average power femtosecond optical parametric oscillator with an additional intracavity focus where signal second harmonic generating crystal is placed. Either OPO, or second intracavity SHG crystal mismatching leads to negative CQN which can be exploited for soliton generation in a positive GDD resonator to generate pulses with minimum time-bandwidth product. The mode of OPO crystal mismatching leads to a simple approach, with a cost of higher power losses, coupled amplification / nonlinearity, spatial beam position walk-off when crystal is tuned. Decoupling of optical parametric amplification part and negative nonlinearity with an additional SHG crystal allows independent control of both of these parameters to operate in a solitonic regime with varying wavelength. Throughout the wavelength tuning range, the time bandwidth product <0.6 and pulse durations <200 fs were demonstrated while the CQN induced average power losses were less than 20% with peak power conserved. Two crystal approach leads to a two-fold improvement: quasi passive output beam stabilization while both crystals are rotated in opposite directions as wavelength is changed; a way to compensate for varying levels of the resonator intracavity group delay dispersion (GDD offsets of +/- 1000 fs^2 with +/- 5% SHG power losses) with negligible beam position drift. These results pave a way for all positive group delay dispersion, broadly wavelength tunable, compact and stable femtosecond optical parametric oscillator as a source for multiphoton imaging application.

Funding

Lietuvos Mokslo Taryba (01.2.2-LMT-K-718-01-0014).

Disclosures

I. Stasevičius and M. Vengris (part-time) are paid employees of “Light Conversion”, Vilnius, Lithuania.

References

1. G. M. Gale, M. Cavallari, and F. Hache, “Femtosecond visible optical parametric oscillator,” J. Opt. Soc. Am. B **15**(2), 702–714 (1998).
2. M. Ghotbi, A. Esteban-Martin, and M. Ebrahim-Zadeh, “BiB_3O_6 femtosecond optical parametric oscillator,” Opt. Lett. **31**(21), 3128–3130 (2006).
3. J. Hebling, E. J. Mayer, J. Kuhl, and R. Szipocs, “Chirped-mirror dispersion-compensated femtosecond optical parametric oscillator,” Opt. Lett. **20**(8), 919–921 (1995).

Optics EXPRESS

4. T. Gottschall, J. Limpert, and A. Tunnermann, "Ultra-short pulse fiber optical parametric oscillator," Opt. Lett. **42**(17), 3423–3426 (2017).
5. J. Vengelis, I. Stasevicius, K. Stankeviciute, V. Jarutis, R. Grigonis, M. Vengris, and V. Sirutkaitis, "Characteristics of optical parametric oscillators synchronously pumped by second harmonic of femtosecond Yb:KGW laser," Opt. Commun. **338**, 277–287 (2015).
6. R. DeSalvo, D. J. Hagan, M. Sheik-Bahae, G. Stegeman, and W. E. Van Stryland, "Self-focusing and self-defocusing by cascaded second-order effects in KTP," Opt. Lett. **17**(1), 28–30 (1992).
7. C. Conti, S. Trillo, G. Gallot, G. M. Gale, P. Di Trapani, J. Kilius, A. Bramati, S. Minardi, W. Chinaglia, and G. Valiulis, "Effective lensing effects in parametric frequency conversion," J. Opt. Soc. Am. B **19**(4), 852–859 (2002).
8. I. Stasevicius, G. Martynaitis, and M. Vengris, "Cascaded nonlinearities in high-power femtosecond optical parametric oscillator," J. Opt. Soc. Am. B **37**(3), 721–729 (2020).
9. I. Ricciardi, S. Mosca, M. Parisi, F. Leo, T. Hansson, M. Erkintalo, P. Maddaloni, P. D. Natale, S. Wabnitz, and M. D. Rosa, "Optical Frequency Combs in Quadratically Nonlinear Resonators," Micromachines **11**(2), 230 (2020).
10. R. Šuminas, G. Tamošauskas, V. Jukna, A. Couairon, and A. Dubietis, "Second-order cascading-assisted filamentation and controllable supercontinuum generation in birefringent crystals," Opt. Express **25**(6), 6746–6756 (2017).
11. H. Guo, B. Zhou, M. Steinert, F. Setzpfandt, T. Pertsch, H. Chung, Y. Chen, and M. Bache, "Supercontinuum generation in quadratic nonlinear waveguides without quasi-phase matching," Opt. Lett. **40**(4), 629–632 (2015).
12. V. Ulvila, C. R. Phillips, L. Halonen, and M. Vainio, "Frequency comb generation by a continuous-wave pumped optical parametric oscillator based on cascading quadratic nonlinearities," Opt. Lett. **38**(21), 4281–4284 (2013).
13. F. Saltarelli, A. Diebold, I. J. Graumann, C. R. Phillips, and U. Keller, "Self-phase modulation cancellation in a high-power ultrafast thin-disk laser oscillator," Optica **5**(12), 1603–1606 (2018).
14. A. S. Mayer, C. R. Phillips, and U. Keller, "Watt-level 10-gigahertz solid-state laser enabled by self-defocusing nonlinearities in an aperiodically poled crystal," Nat. Commun. **8**(1), 1673 (2017).
15. L. J. Qian, X. Liu, and F. W. Wise, "Femtosecond Kerr-lens mode locking with negative nonlinear phase shifts," Opt. Lett. **24**(3), 166–168 (1999).
16. G. Cerullo, S. D. Silvestri, A. Monguzzi, D. Segala, and V. Magni, "Self-starting mode locking of a cw Nd:YAG laser using cascaded second-order nonlinearities," Opt. Lett. **20**(7), 746–748 (1995).
17. S. T. Lin and C.-H. Huang, "Effects of nonlinear phase in cascaded mode-locked Nd: YVO_4 laser," Opt. Express **27**(2), 504–511 (2019).
18. R. Laenen, H. Graener, and A. Laubereau, "Evidence for chirp reversal and self-compression in a femtosecond optical parametric oscillator," J. Opt. Soc. Am. B **8**(5), 1085–1088 (1991).
19. F. Hache, A. Zeboulon, G. Gallot, and G. M. Gale, "Cascaded second-order effects in the femtosecond regime in β-barium borate: self-compression in a visible femtosecond optical parametric oscillator," Opt. Lett. **20**(14), 1556–1558 (1995).
20. A. E. Siegman, *Lasers* (University Science Books, 1986).
21. O. E. Martinez, "Matrix Formalism for Dispersive Laser Cavities," IEEE J. Quantum Electron. **25**(3), 296–300 (1989).
22. G. P. Agrawal, *Nonlinear Fiber Optics 5th Edition* (Academic Press, 2013).
23. J. Bromage, J. Rothhardt, S. Hadrich, C. Dorrer, C. Jocher, S. Demmler, J. Limpert, A. Tunnermann, and J. D. Zuegel, "Analysis and suppression of parasitic processes in noncollinear optical parametric amplifiers," Opt. Express **19**(18), 16797–16808 (2011).
24. D. Nikogosyan, *Nonlinear Optical Crystals: A Complete Survey* (Springer, 2015).
25. S. Zahedpour, J. K. Wahlstrand, and H. M. Milchberg, "Measurement of the nonlinear refractive index of air constituents at mid-infrared wavelengths," Opt. Lett. **40**(24), 5794–5797 (2015).
26. M. Bache, O. Bang, W. Krolikowski, J. Moses, and F. W. Wise, "Limits to compression with cascaded quadratic soliton compressors," Opt. Express **16**(5), 3273–3287 (2008).
27. K. C. Burr, C. L. Tang, M. A. Arbore, and M. M. Fejer, "Broadly tunable mid-infrared femtosecond optical parametric oscillator using all-solid-state-pumped periodically poled lithium niobate," Opt. Lett. **22**(19), 1458–1460 (1997).

193.219.55.139 (ta 2021-04-29 03:09:44)